GEOPHYSICS, VOL. 71, NO. 6 (NOVEMBER-DECEMBER 2006); P. G333–G345, 21 FIGS., 3 TABLES.
10.1190/1.2358403

Downloaded 12/18/15 to 132.239.1.230. Redistribution subject to SEG license or copyright; see Terms of Use at http://library.seg.org/

Integral equation method for 3D modeling of electromagnetic fields in complex structures with inhomogeneous background conductivity

Michael S. Zhdanov[1], Seong Kon Lee[2], and Ken Yoshioka[1]

ABSTRACT

We present a new formulation of the integral equation (IE) method for three-dimensional (3D) electromagnetic (EM) modeling in complex structures with inhomogeneous background conductivity (IBC). This method overcomes the standard limitation of the conventional IE method related to the use of a horizontally layered background only. The new 3D IE EM modeling method still employs the Green's functions for a horizontally layered 1D model. However, the new method allows us to use an inhomogeneous background with the IE method. We also introduce an approach for accuracy control of the IBC IE method. This new approach provides us with the ability to improve the accuracy of computations by applying the IBC technique iteratively. This approach seems to be extremely useful in computing EM data for multiple geologic models with some common geoelectrical features, like terrain, bathymetry, or other known structures. It may find wide application in an inverse problem solution, where we have to keep some known geologic structures unchanged during the iterative inversion. The method was carefully tested for modeling the EM field for complex structures with a known variable background conductivity. The effectiveness of this approach is illustrated by modeling marine controlled-source electromagnetic (MCSEM) data in the area of Gemini Prospect, Gulf of Mexico.

INTRODUCTION

The integral equation (IE) method is an important tool in three-dimensional (3D) electromagnetic (EM) modeling for geophysical applications. It was introduced originally in a pioneer paper by Dmitriev (1969), which was published in Russian and long remained unknown to Western geophysicists (as well as was the work of Tabarovsky, 1975). Almost 30 years ago, practically simultaneously, Raiche (1974), Weidelt (1975), and Hohmann (1975) published their famous papers on the IE method. Many more researchers have contributed to the improvement and development of this method in recent years (e.g., Wannamaker, 1991; Dmitriev and Nesmeyanova, 1992; Xiong, 1992; Xiong and Kirsch, 1992; Singer and Fainberg, 1997; Avdeev et al., 2002; Hursán and Zhdanov, 2002; Zhdanov, 2002; Singer et al., 2003; Abubakar and van der Berg, 2004; Avdeev, 2005; Yoshioka and Zhdanov, 2005).

In the framework of the IE method, the conductivity distribution is divided into two parts: (1) the background conductivity σ_b, which is used for the Green's functions calculation, and (2) the anomalous conductivity $\Delta\sigma_a$ within the domain of integration D. It was emphasized in the original paper by Dmitriev (1969) that the main limitation of the IE method is that the background conductivity model must have a simple structure to allow for an efficient Green's function calculation. The most widely used background models in EM exploration are those formed by horizontally homogeneous layers. The theory of the Green's functions for layered one-dimensional (1D) models is very well developed and lays the foundation for efficient numerical algorithms. Any deviation from this 1D background model must be treated as an anomalous conductivity.

In some practical applications, however, it is difficult to describe a model using horizontally layered background conductivity. As a result, the domain of integration may become too large, which increases significantly the size of the modeling domain and of the required computer memory and computational time for IE modeling. We will be able to overcome these computational difficulties if the IE method will allow us to use variable background conductivity. This will also be helpful in modeling EM data for multiple geologic models with some common geoelectrical features, like known topographic or bathymetric inhomogeneities (in the case of marine EM) or salt dome structures. The conventional approach would require us to run the full 3D IE method for all domains with the anomalous conductiv-

Manuscript received by the Editor June 30, 2005; revised manuscript received July 12, 2006; published online November 3, 2006.
[1]University of Utah, Department of Geology and Geophysics, 135 South 1460 East, Room 719, Salt Lake City, Utah 84112. E-mail: mzhdanov@mines.utah.edu.
[2]Korea Institute of Geoscience and Mineral Resources, Groundwater and Geothermal Resources Division, 30 Gajeong-dong, Yuseong-gu, Daejeon 305-350, Korea. E-mail: seongkon@kigam.re.kr.
© 2006 Society of Exploration Geophysicists. All rights reserved.

Downloaded 12/18/15 to 132.239.1.230. Redistribution subject to SEG license or copyright; see Terms of Use at http://library.seg.org/

ity every time we change the parameters within one domain only. This situation occurs, for example, when we have known information about the existence of specific geologic structures that should be considered in modeling and/or inversion (Zhdanov and Wilson, 2004).

In the present paper, we extend the formulation of the IE method to the more general case of models with an inhomogeneous background conductivity (IBC). Our method is based on the separation of the effects related to excess electric current $\mathbf{j}^{\Delta\sigma_b}$, induced in the inhomogeneous background domain, from those effects related to the anomalous electric current $\mathbf{j}^{\Delta\sigma_a}$ in the location of the anomalous conductivity, respectively. As a result, we arrive at a system of integral equations that uses the same simple Green's functions for the layered model as in the original IE formulation. However, the new equations take into account the effect of the variable background conductivity distribution. We also consider an approach to the accuracy control of the IBC IE method. This approach provides us with the ability to improve the accuracy of computations by applying the IBC technique iteratively.

The developed method and numerical code are tested on typical geoelectrical models with the variable background. We also investigate the effectiveness of this approach for modeling marine controlled-source electromagnetic (MCSEM) data in areas with significant bathymetric inhomogeneities. The accurate simulation of the EM field caused by bathymetric inhomogeneities is a challenging numerical problem because it requires a huge number of discretization cells to represent the bathymetric structures properly. The natural choice for solving this problem would be a finite-difference (FD) and/or finite-element (FE) method. However, the FD and FE methods require the discretization of the entire modeling domain, whereas the IE method needs a smaller grid covering the anomalous domain only. As a result, using the same number of discretization cells, the IE method allows a more detailed representation of the complex geology than the FD and/or FE methods. (Note, however, that the matrix of the system of IE equations is full, whereas the matrix of the FD equations is sparse.) Moreover, in the framework of the IBC approach to the construction of the IE method, one can precompute the bathymetry effect only once and keep it unchanged during the entire modeling and/or inversion process. Taking into account that precomputing the bathymetry effect constitutes the most time-consuming part of the forward EM modeling, this approach would allow us to increase the effectiveness of the computer simulation in the interpretation of the MCSEM data significantly. We illustrate this approach by modeling MCSEM data in the area of Gemini Prospect, Gulf of Mexico.

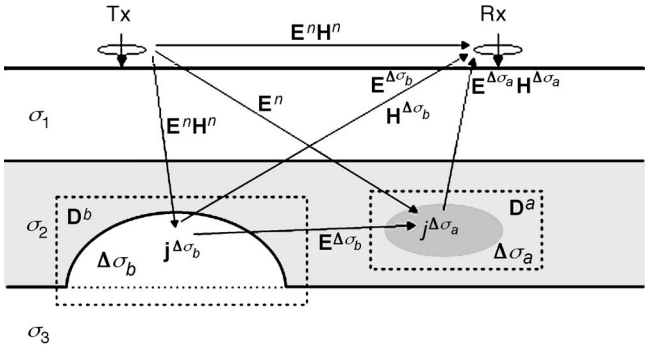

Figure 1. A sketch of a 3D geoelectric model with horizontally layered (normal) conductivity σ_n, inhomogeneous background conductivity $\sigma_b = \sigma_n + \Delta\sigma_b$ within a domain D_b and anomalous conductivity $\Delta\sigma_a$ within a domain D_a. The EM field in this model is a sum of the normal fields $\mathbf{E}^n$ and $\mathbf{H}^n$ generated by the given source(s) in the model with normal distribution of conductivity σ_n, a variable background effect $\mathbf{E}^{\Delta\sigma_b}$ and $\mathbf{H}^{\Delta\sigma_b}$ produced by the inhomogeneous background conductivity $\Delta\sigma_b$ and the anomalous fields $\mathbf{E}^{\Delta\sigma_a}$ and $\mathbf{H}^{\Delta\sigma_a}$ related to the anomalous conductivity distribution, $\Delta\sigma_a$. *T*x = transmitters; *R*x = receiver.

IE METHOD IN A MODEL WITH IBC

We consider a 3D geoelectrical model with horizontally layered (normal) conductivity σ_n, inhomogeneous background conductivity $\sigma_b = \sigma_n + \Delta\sigma_b$ within a domain D_b, and anomalous conductivity $\Delta\sigma_a$ within a domain D_a (Figure 1). The model is excited by an EM field generated from an arbitrary source which is time-harmonic as $e^{-i\omega t}$. The EM field in this model satisfies Maxwell's equations:

$$\nabla \times \mathbf{H} = \sigma_n\mathbf{E} + \mathbf{j} = \sigma_n\mathbf{E} + \mathbf{j}^{\Delta\sigma_b} + \mathbf{j}^{\Delta\sigma_a} + \mathbf{j}^e,$$
$$\nabla \times \mathbf{E} = i\omega\mu_0\mathbf{H}, \tag{1}$$

where

$$\mathbf{j}^{\Delta\sigma_a} = \begin{cases} \Delta\sigma_a\mathbf{E}, & \mathbf{r} \in D_a \\ 0, & \mathbf{r} \notin D_a \end{cases} \tag{2}$$

is the anomalous current within the local inhomogeneity D_a and

$$\mathbf{j}^{\Delta\sigma_b} = \begin{cases} \Delta\sigma_b\mathbf{E}, & \mathbf{r} \in D_b \\ 0, & \mathbf{r} \notin D_b \end{cases} \tag{3}$$

is the excess current within the inhomogeneous background domain D_b.

Equations 1–3 show that one can represent the EM field in this model as a sum of the normal fields $\mathbf{E}^n$ and $\mathbf{H}^n$ generated by the given source(s) in the model with normal distribution of conductivity σ_n, a variable background effect $\mathbf{E}^{\Delta\sigma_b}$ and $\mathbf{H}^{\Delta\sigma_b}$ produced by the inhomogeneous background conductivity $\Delta\sigma_b$ and the anomalous fields $\mathbf{E}^{\Delta\sigma_a}$ and $\mathbf{H}^{\Delta\sigma_a}$ related to the anomalous conductivity distribution $\Delta\sigma_a$:

$$\mathbf{E} = \mathbf{E}^n + \mathbf{E}^{\Delta\sigma_b} + \mathbf{E}^{\Delta\sigma_a}, \quad \mathbf{H} = \mathbf{H}^n + \mathbf{H}^{\Delta\sigma_b} + \mathbf{H}^{\Delta\sigma_a}. \tag{4}$$

The total EM field in this model can be written as

$$\mathbf{E} = \mathbf{E}^b + \mathbf{E}^{\Delta\sigma_a}, \quad \mathbf{H} = \mathbf{H}^b + \mathbf{H}^{\Delta\sigma_a}, \tag{5}$$

where the background EM field $\mathbf{E}^b$, $\mathbf{H}^b$ is a sum of the normal fields and those caused by the inhomogeneous background conductivity:

$$\mathbf{E}^b = \mathbf{E}^n + \mathbf{E}^{\Delta\sigma_b}, \quad \mathbf{H}^b = \mathbf{H}^n + \mathbf{H}^{\Delta\sigma_b}. \tag{6}$$

Following the standard logic of the IE method (Zhdanov, 2002), we write the integral representations for the EM fields of the given current distribution,

$$\mathbf{j}^{\Delta\sigma}(\mathbf{r}) = \mathbf{j}^{\Delta\sigma_b}(\mathbf{r}) + \mathbf{j}^{\Delta\sigma_a}(\mathbf{r}) = \Delta\sigma_b\mathbf{E}(\mathbf{r}) + \Delta\sigma_a\mathbf{E}(\mathbf{r}),$$

within a medium of normal conductivity σ_n:

$$\mathbf{E}(\mathbf{r}_j) = \mathbf{E}^n + \iiint_{D_b} \hat{\mathbf{G}}_E(\mathbf{r}_j|\mathbf{r}) \cdot \Delta\sigma_b\mathbf{E}(\mathbf{r})dv$$

$$+\iiint_{D_a}\hat{\mathbf{G}}_E(\mathbf{r}_j|\mathbf{r})\cdot\Delta\sigma_a\mathbf{E}(\mathbf{r})dv,$$

$$\mathbf{H}(\mathbf{r}_j)=\mathbf{H}^n+\iiint_{D_b}\hat{\mathbf{G}}_H(\mathbf{r}_j|\mathbf{r})\cdot\Delta\sigma_b\mathbf{E}(\mathbf{r})dv+\iiint_{D_a}\hat{\mathbf{G}}_H(\mathbf{r}_j|\mathbf{r})\cdot\Delta\sigma_a\mathbf{E}(\mathbf{r})dv, \quad (7)$$

where the first integral terms describe the excess part of the background fields generated by the excess currents in the inhomogeneous background domain D_b:

$$\mathbf{E}^{\Delta\sigma_b}(\mathbf{r}_j)=\iiint_{D_b}\hat{\mathbf{G}}_E(\mathbf{r}_j|\mathbf{r})\cdot\Delta\sigma_b\mathbf{E}(\mathbf{r})dv=\mathbf{G}_E^{D_b}(\Delta\sigma_b\mathbf{E}), \quad (8)$$

$$\mathbf{H}^{\Delta\sigma_b}(\mathbf{r}_j)=\iiint_{D_b}\hat{\mathbf{G}}_H(\mathbf{r}_j|\mathbf{r})\cdot\Delta\sigma_b\mathbf{E}(\mathbf{r})dv=\mathbf{G}_H^{D_b}(\Delta\sigma_b\mathbf{E}). \quad (9)$$

The second terms describe the anomalous fields generated by the anomalous domain D_a:

$$\mathbf{E}^{\Delta\sigma_a}(\mathbf{r}_j)=\mathbf{E}(\mathbf{r}_j)-\mathbf{E}^n(\mathbf{r}_j)-\mathbf{E}^{\Delta\sigma_b}(\mathbf{r}_j)=\iiint_{D_a}\hat{\mathbf{G}}_E(\mathbf{r}_j|\mathbf{r})\cdot\Delta\sigma_a\mathbf{E}(\mathbf{r})dv=\mathbf{G}_E^{D_a}(\Delta\sigma_a\mathbf{E}), \quad (10)$$

$$\mathbf{H}^{\Delta\sigma_a}(\mathbf{r}_j)=\mathbf{H}(\mathbf{r}_j)-\mathbf{H}^n(\mathbf{r}_j)-\mathbf{H}^{\Delta\sigma_b}(\mathbf{r}_j)=\iiint_{D_a}\hat{\mathbf{G}}_H(\mathbf{r}_j|\mathbf{r})\cdot\Delta\sigma_a\mathbf{E}(\mathbf{r})dv=\mathbf{G}_H^{D_a}(\Delta\sigma_a\mathbf{E}). \quad (11)$$

In equations 8–11, the symbols $\mathbf{G}_E^{D_a,D_b}$ and $\mathbf{G}_H^{D_a,D_b}$ denote the electric and magnetic Green's operators with a volume integration of D_a or D_b, respectively. Note that according to notation 6, equations 10 and 11 can be rewritten in the form

$$\mathbf{E}^{\Delta\sigma_a}(\mathbf{r}_j)=\mathbf{E}(\mathbf{r}_j)-\mathbf{E}^n(\mathbf{r}_j)-\mathbf{E}^{\Delta\sigma_b}(\mathbf{r}_j)=\mathbf{G}_E^{D_a}(\Delta\sigma_a(\mathbf{E}^b+\mathbf{E}^{\Delta\sigma_a})), \quad (12)$$

$$\mathbf{H}^{\Delta\sigma_a}(\mathbf{r}_j)=\mathbf{H}(\mathbf{r}_j)-\mathbf{H}^n(\mathbf{r}_j)-\mathbf{H}^{\Delta\sigma_b}(\mathbf{r}_j)=\mathbf{G}_H^{D_a}(\Delta\sigma_a(\mathbf{E}^b+\mathbf{E}^{\Delta\sigma_a})). \quad (13)$$

Using integral equations 12 and 13, one can calculate the EM field at any point $\mathbf{r}_j$ if the electric field is known within the inhomogeneity. Equation 12 becomes the integral equation for the electric field $\mathbf{E}(\mathbf{r})$ if $\mathbf{r}_j\in D_a$.

The basic idea of a new IE formulation is that we can take into account the EM field induced in the anomalous domain by the excess currents in the background inhomogeneity $\mathbf{j}^{\Delta\sigma_b}$ but would ignore the return induction effects by the anomalous currents $\mathbf{j}^{\Delta\sigma_a}$. In other words, we assume that the anomalous electric fields $\mathbf{E}^{\Delta\sigma_a}$ are much smaller than the background fields $\mathbf{E}^b$ inside the domain of integration D_b in equations 8 and 9:

$$\mathbf{E}^{\Delta\sigma_b}(\mathbf{r}_j)\approx\mathbf{G}_E^{D_b}(\Delta\sigma_b\mathbf{E}^b)=\mathbf{G}_E^{D_b}(\Delta\sigma_b(\mathbf{E}^n+\mathbf{E}^{\Delta\sigma_b})), \quad (14)$$

$$\mathbf{H}^{\Delta\sigma_b}(\mathbf{r}_j)\approx\mathbf{G}_H^{D_b}(\Delta\sigma_b\mathbf{E}^b)=\mathbf{G}_H^{D_b}(\Delta\sigma_b(\mathbf{E}^n+\mathbf{E}^{\Delta\sigma_b})). \quad (15)$$

Equations 14 and 15 show that finding the excess part of the background fields requires solving the conventional IE for the electric fields in media with inhomogeneous background conductivity distribution (without the anomalous domain D_a). Therefore, we can calculate the background fields using equations 6 and substitute it into equations 12 and 13. The last system of the equations can be solved using the standard IE approach as well.

We should note that the technique outlined above is very different from the conventional Born approximation because we solve the corresponding integral equations 14 and 15 with respect to the anomalous field. With the Born approximation, one does not solve any integral equation. Instead, the background field is just integrated over the domain with the anomalous conductivity (anomalous domain D_a in our case). In our approach, when we solve the first integral equation for the background field, we ignore the secondary field in the inhomogeneous background domain D_b, owing to the return induction effects of the anomalous currents $\mathbf{j}^{\Delta\sigma_a}$ induced in the anomalous domain D_a only. The effect of this secondary field is assumed to be very small compared with the normal field and the secondary field induced in the inhomogeneous background itself. We will discuss in the next section a technique for the accuracy control of this condition.

Another important question is how the IBC should be selected. We recommend that the regional geoelectrical structures should be included in the inhomogeneous background, whereas the local geologic target (e.g., a petroleum reservoir) should be associated with the domain with the anomalous conductivity. At the same time, it is reasonable to include in the IBC model some known geologic structures, such as known topographic or bathymetric inhomogeneities (in the case of marine EM) or a salt dome, to reduce the modeling domain to the area of investigation only.

ACCURACY CONTROL OF THE IBC IE METHOD

We have demonstrated above that the IBC IE method is based on an idea that we can ignore a secondary field induced by the currents in the anomalous domain D_a when we solve the integral equation 14 for the background field $\mathbf{E}^b$ in the domain D_b. The assumption is that this returned induction field is very small compared to the normal field and with an anomalous part of the background field induced in the background conductivity. The obvious condition where this approximation can be employed is that the effect of the induced field $\mathbf{G}_E^{D_b}(\Delta\sigma_b(\mathbf{E}^{\Delta\sigma_a}))$ in inhomogeneous background from the anomalous body is much smaller than the effect of the background field itself inside the domain of integration D_b:

$$\|\mathbf{E}^b-\mathbf{G}_E^{D_b}(\Delta\sigma_b(\mathbf{E}^b+\mathbf{E}^{\Delta\sigma_a}))-\mathbf{E}^n\|_{D_b}/\|\mathbf{E}^b\|_{D_b}=\varepsilon_1^b\ll 1, \quad (16)$$

where $\|\ldots\|_{D_b}$ denotes the l_2-norm calculated over domain D_b:

Downloaded 12/18/15 to 132.239.1.230. Redistribution subject to SEG license or copyright; see Terms of Use at http://library.seg.org/

$$\|\mathbf{E}^b\|^2_{D_b} = \iiint_{D_b} |\mathbf{E}^b(\mathbf{r})|^2 dv.$$

We can also evaluate the possible errors of ignoring the return response of the currents induced in the inhomogeneous background on the field in the anomalous domain D_a:

$$\|\mathbf{E}^a - \mathbf{G}_E^{D_a}(\Delta\sigma_a(\mathbf{E}^a + \mathbf{E}^{\Delta\sigma_b(1)})) - \mathbf{E}^n\|_{D_a} / \|\mathbf{E}^a\|_{D_a} = \varepsilon_1^a, \quad (17)$$

where

$$\mathbf{E}^{\Delta\sigma_b(1)}(\mathbf{r}_j) = \mathbf{G}_E^{D_b}(\Delta\sigma_b(\mathbf{E}^b + \mathbf{E}^{\Delta\sigma_a})), \quad \mathbf{r}_j \in D_a$$

and

$$\mathbf{E}^a = \mathbf{E}^n + \mathbf{E}^{\Delta\sigma_a}.$$

A simple observation based on formulas 16 and 17 is that the accuracy of the IBC IE method should depend on the electrical distance between a domain with the IBC and an anomalous domain $r_\lambda = r/\lambda$, where r is a geometric distance and λ is a corresponding wavelength in the layered background. The larger this distance is, the smaller is the return effect of the currents induced in the anomalous domain on the IBC domain and vice versa. However, our modeling study shows that even in the case of the anomalous domain attached to the IBC domain, we still have a reasonable accuracy of the IBC IE method (see Model 3 below). In addition, we should note that the accuracy of the IBC IE method should also depend on the shape and relative aspect of the domains D_a and D_b.

Condition 16 makes it possible to evaluate the accuracy of the IBC IE method in a general case compared with the conventional IE method. Indeed, one can apply the IE method for the computations of the background field $\mathbf{E}^b$ and the anomalous field $\mathbf{E}^{\Delta\sigma_a}$ using two separate integral equations, 12 and 14. After that, we can evaluate the possible error in the background field computations ε_1^b and in the anomalous field calculations ε_1^a using the proposed technique.

The remarkable fact is that the above condition not only provides us with the ability to control the accuracy of our computations but it also shows us how to improve the accuracy by applying the IBC technique iteratively. Indeed, if we find that the error ε_1^b is too large, we can solve the rigorous integral equation 8 for the background electric field, considering the anomalous field $\mathbf{E}^{\Delta\sigma_a}$ computed in the previous step:

$$\mathbf{E}^b(\mathbf{r}_j) = \mathbf{G}_E^{D_b}(\Delta\sigma_b(\mathbf{E}^b + \mathbf{E}^{\Delta\sigma_a})) + \mathbf{E}^n(\mathbf{r}_j), \quad \mathbf{r}_j \in D_b. \quad (18)$$

We denote by $\mathbf{E}^{b(2)}$ a solution of equation 18. Now we can use this updated background field $\mathbf{E}^{b(2)}$ in integral equation 12 for the anomalous field:

$$\mathbf{E}^{\Delta\sigma_a}(\mathbf{r}_j) = \mathbf{G}_E^{D_a}(\Delta\sigma_a(\mathbf{E}^{b(2)} + \mathbf{E}^{\Delta\sigma_a})), \quad \mathbf{r}_j \in D_a. \quad (19)$$

A solution of the last equation gives us a second iteration of the anomalous electric field $\mathbf{E}^{\Delta\sigma_a(2)}$.

We can check the accuracy of the second round of the IBC IE method for domains D_a and D_b using the following estimates, respectively:

$$\|\mathbf{E}^{a(2)} - \mathbf{G}_E^{D_a}(\Delta\sigma_a(\mathbf{E}^{a(2)} + \mathbf{E}^{\Delta\sigma_b(2)}) - \mathbf{E}^n)\|_{D_a} / \|\mathbf{E}^{a(2)}\|_{D_a} = \varepsilon_2^a,$$
$$\|\mathbf{E}^{b(2)} - \mathbf{G}_E^{D_b}(\Delta\sigma_b(\mathbf{E}^{b(2)} + \mathbf{E}^{\Delta\sigma_a(2)}) - \mathbf{E}^n)\|_{D_b} / \|\mathbf{E}^{b(2)}\|_{D_b} = \varepsilon_2^b, \quad (20)$$

where

$$\mathbf{E}^{a(2)} = \mathbf{E}^n + \mathbf{E}^{\Delta\sigma_a(2)}$$

and

$$\mathbf{E}^{\Delta\sigma_b(2)}(\mathbf{r}_j) = \mathbf{G}_E^{D_b}(\Delta\sigma_b(\mathbf{E}^{b(2)} + \mathbf{E}^{\Delta\sigma_a(2)})),$$

$$\mathbf{r}_j \in D_a.$$

The iterative process described above is continued until we reach the required accuracy of the background field calculations in both D_a and D_b. We should note in conclusion that this iterative process always converges because we use the contraction integral equation (CIE) method of Hursán and Zhdanov (2002) as a main algorithm for the solution of the corresponding EM field integral equations 14 and 12.

SYNTHETIC MODEL EXAMPLES

The CIE method was implemented in the INTEM3D code, developed by the Consortium for Electromagnetic Modeling and Inversion (CEMI) (Hursán and Zhdanov, 2002). A new version of the IE code, IBCEM3D (inhomogeneous background conductivity 3D EM modeling) has been developed based on the original INTEM3D code (Zhdanov and Lee, 2005). This code includes the following modifications of the original INTEM3D code:

1) Includes an additional stage in the IBCEM3D code of computing the corresponding Green's tensors from the cells of the domain D_b to the receivers and to the cells of the domain D_3;
2) Precomputes the background electric field in the receivers and in the cells of the modeling grid within the domain D_a of the anomalous conductivity for a model with variable background. Computations are done using the model which contains only background inhomogeneities $\sigma_b = \sigma_n + \Delta\sigma_b$ and no anomalous conductivity $\Delta\sigma_a = 0$;
3) Substitutes the normal electric field $\mathbf{E}^n$ with a new background field $\mathbf{E}^b$ precomputed on the previous stage and solves the integral equation 12.

Note that the new code, IBCEM3D, can be used for modeling the EM field generated by different sources in complex 3D geoelectrical structures. The sources used in the program are the same as in INTEM3D:

- plane wave propagating vertically toward the earth (magnetotelluric)
- current bipoles along the x-, y-, and z-directions
- horizontal rectangular loop
- horizontal circular loop
- moving horizontal loops
- magnetic dipoles oriented in the x-, y-, and z-directions.

The new algorithm and the computer code have been verified on a set of test models with inhomogeneous background conductivity.

Downloaded 12/18/15 to 132.239.1.230. Redistribution subject to SEG license or copyright; see Terms of Use at http://library.seg.org/

Downloaded 12/18/15 to 132.239.1.230. Redistribution subject to SEG license or copyright; see Terms of Use at http://library.seg.org/

Model 1: Validity of the inhomogeneous background algorithm

We have applied the inhomogeneous background conductivity algorithm (IBCEM3D) to a simple numerical model to analyze its overall efficiency in comparison with conventional IE modeling. The results of conventional IE modeling are obtained by INTEM3D (Hursán and Zhdanov, 2002). Figure 2 shows a sketch of Model 1 selected for this modeling experiment. Two conductive cubic bodies, A and B, are embedded in a homogeneous half-space. The resistivity of the bodies is 10 ohm-m and that of the homogenous background is 100 ohm-m. The cubic bodies have a side of 400 m. They are located at a depth of 200 m below the surface at a distance of 400 m, one from another, as shown in Figure 2. This example provides a very simple but useful test of the new method because it represents an extreme situation where there is no apparent difference between the inhomogeneous background, represented by one body, and the anomalous domain, represented by another body. One would suspect that ignoring a return effect from one body to another body of a similar size would produce a significant error. However, this example shows that the method developed in our paper works surprisingly well in this extreme situation.

We have computed the EM responses for this model in 441 receivers located at every 100 m in the x- and y-direction of a 21×21 grid using both the original INTEM3D algorithm and the new IBCEM3D code. We have noted above that the new code can be used for modeling the EM field generated by different sources. In our numerical test, we have simulated the EM field generated by a vertically propagated plane EM wave [magnetotelluric (MT) data simulation]. The plane waves in two H- and E-polarizations are used as the sources with the number of frequencies, equal to 21, equally logarithmically spaced from 0.01 to 1000 Hz. We use the biconjugate gradient stabilized (BICGSTAB) subroutine (Hursán and Zhdanov, 2002) to solve the system of linear IE equations, and the desired misfit level of the matrix solution is 10^{-5} in both modeling experiments. In the inhomogeneous background algorithm, the inhomogeneous background is formed by the homogeneous earth and body B. The conventional INTEM3D code uses just the homogeneous half-space as a background.

Figures 3 and 4 show the real and imaginary components of the sum of electric fields $E_x^{\Delta\sigma_b}$ and $E_x^{\Delta\sigma_a}$ and magnetic fields $H_y^{\Delta\sigma_a}$ and $H_y^{\Delta\sigma_b}$ for H-polarization, computed using two different codes. The profile is along the x-axis at $y = 0$. The solid lines represent the results obtained by the conventional IE method (INTEM3D), whereas the circles represent those computed using a new inhomogeneous background algorithm (IBCEM3D). One can see that both results agree well with each other for the entire frequency range used in this analysis.

First of all, we have analyzed the accuracy of our forward modeling using formulas 16 and 17. One can see from Table 1 that, even for this extreme case where we have two identical bodies, A and B, the relative errors ε_1^b of ignoring the secondary field generated in domain D_b (body B) by the anomalous currents induced in domain D_a (body A) do not exceed 16% for H-polarization and 9% for E-polarization, respectively. At the same time, the relative errors ε_1^a of ignoring the return response of these additional currents within domain D_b (body B) on the field in domain D_a (body A) do not exceed 1% for H-polarization and 0.4% for E-polarization, respectively. The errors are larger for H-polarization than for E-polarization, which can be explained by the fact that, in the case of H-polarization, there is slightly stronger galvanic coupling between two bodies than in the case of E-polarization.

To compare the responses in detail, Figures 5 and 6 present the differences (errors) between the results obtained by the two algorithms. Note that the errors presented in Table 1 provide an integrated accuracy evaluation for entire modeling domains, D_a and D_b, respective-

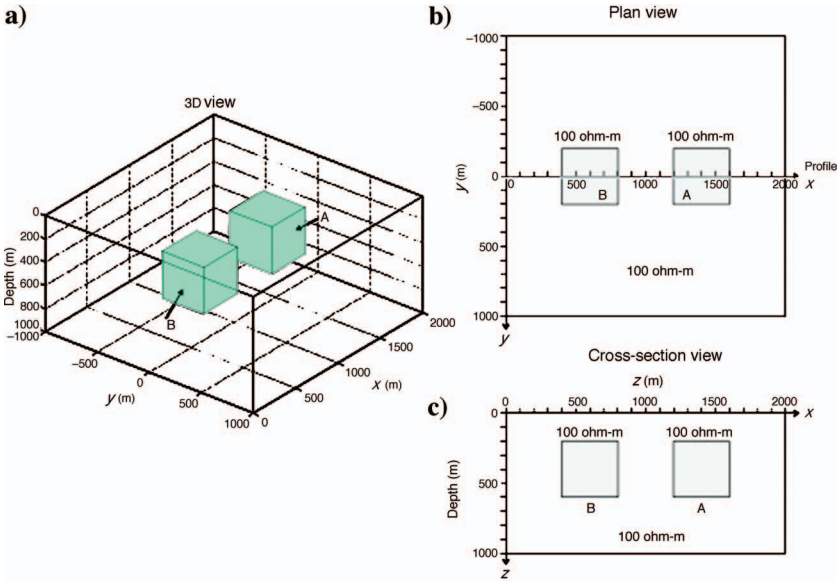

Figure 2. A sketch of Model 1 used to test the validity of an inhomogeneous background algorithm. Two cubic conductors of the same size and conductivity are embedded in a homogeneous background. (a) 3D view, (b) plan view, and (c) vertical cross section of Model 1.

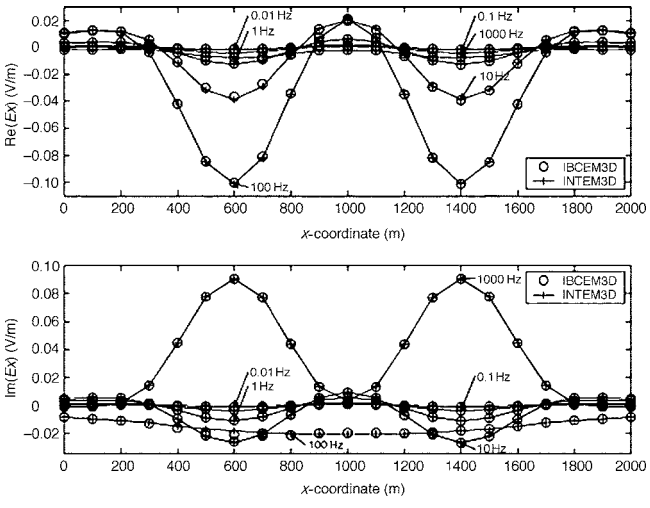

Figure 3. Plots of the real and imaginary parts of the sum of electric fields $E_x^{\Delta\sigma_b}$ and $E_x^{\Delta\sigma_a}$ along the x-directed profile at $y = 0$. The solid lines represent the results obtained by the conventional IE method (INTEM3D); the circles show the data computed using a new inhomogeneous background algorithm (IBCEM3D).

Downloaded 12/18/15 to 132.239.1.230. Redistribution subject to SEG license or copyright; see Terms of Use at http://library.seg.org/

ly, whereas the errors shown in Figures 5 and 6 represent the local errors in the observation points. At the same time, in full accord with Table 1, these errors slightly increase above body B, but they are almost equal to zero above body A. This is because our method takes into account the EM field induced in the anomalous domain (body A) by the excess currents in the background inhomogeneity (body B), but it ignores the return induction effect on body B of the anomalous currents in body A. The maximum normalized errors, however, are less than 3% in E_x and 5% in H_y for H-polarization within the entire frequency range considered in this example. This is actually a very good property of the developed method. Indeed, we propose to use this method for modeling and/or inversion of the EM data in geoelectrical structures with known and fixed IBC but with a changing (or unknown in inversion) anomalous conductivity. In this situation, it is more important to have an accurate calculation of the data in the area of the anomalous conductivity distributions than over the known background.

Finally, we have computed the EM field for this model using Born approximation for comparison (Figures 7 and 8). The results show the huge errors (several hundred percent) produced by the Born approximation, whereas the method introduced in our paper generates a very accurate result. This example demonstrates once again that there is a principal difference between the IBC method and the conventional Born approximation. In the case of the Born approximation, one does not solve any integral equation. The background field is just integrated over the domain with the anomalous conductivity. Contrary to the Born approximation, in the framework of the IBC method, we ignore the return effect in the inhomogeneous background from the anomalous domain only, while solving a corresponding integral equation for the anomalous field in the anomalous domain. As a result, we obtain very accurate values of the anomalous EM field.

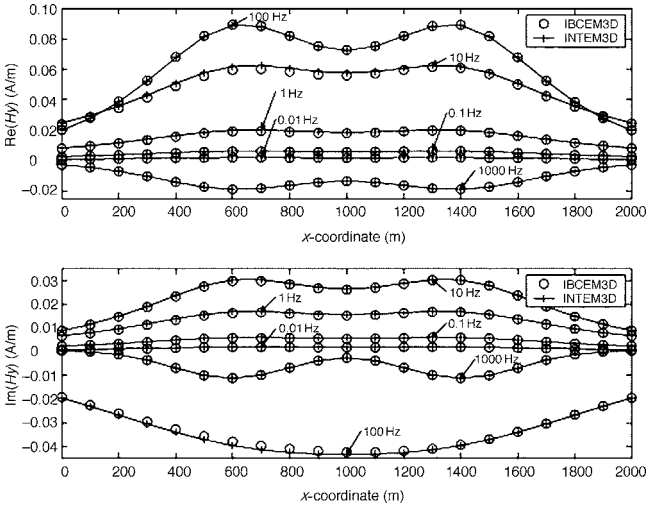

Figure 4. Plots of the real and imaginary parts of the sum of magnetic fields $H_y^{\Delta\sigma_b}$ and $H_y^{\Delta\sigma_a}$ along the x-directed profile at $y = 0$ calculated for Model 1. The solid lines represent the results obtained by INTEM3D; the circles show the data computed by IBCEM3D.

Table 1. Accuracy of IBC IE method for Model 1. The value ε_1^b denotes the relative errors of ignoring the secondary field generated in domain D_b by the anomalous currents induced in domain D_a; ε_1^a denotes the relative errors of ignoring the return response of these additional currents within domain D_b on the field in domain D_a. The abbreviation pol. is polarization.

Frequency Hz	ε_1^b H-pol.	ε_1^b E-pol.	$\varepsilon_1^a H$-pol.	$\varepsilon_1^a E$-pol.
0.01	0.156	0.089	0.012	0.004
0.1	0.156	0.089	0.011	0.004
1	0.156	0.089	0.011	0.004
10	0.148	0.094	0.010	0.004
100	0.084	0.106	0.003	0.005
1000	0.006	0.025	0.0003	0.0004

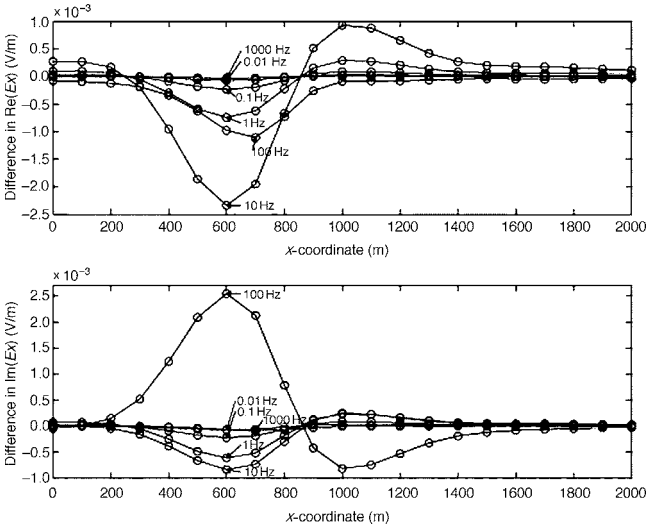

Figure 5. Model 1. Plots of the differences (errors) between the results obtained by two algorithms, INTEM3D and IBCEM3D, for the real and imaginary parts of the sum of electric fields $E_x^{\Delta\sigma_b}$ and $E_x^{\Delta\sigma_a}$ along an x-directed profile at $y = 0$.

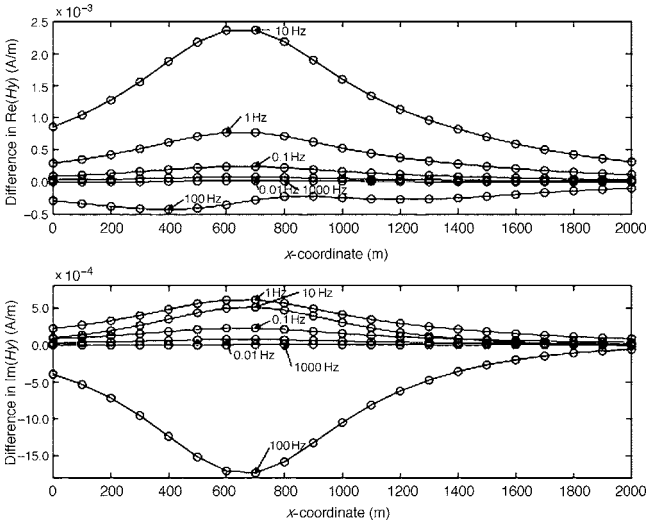

Figure 6. Model 1. Plots of the differences (errors) between the results obtained by two algorithms, INTEM3D and IBCEM3D, for the real and imaginary parts of magnetic fields $H_y^{\Delta\sigma_b}$ and $H_y^{\Delta\sigma_a}$ along an x-directed profile at $y = 0$.

Downloaded 12/18/15 to 132.239.1.230. Redistribution subject to SEG license or copyright; see Terms of Use at http://library.seg.org/

We have compared the computational time required by both algorithms for this model in a Matlab 7.0 environment running on a PC equipped with Intel Pentium 4 3.6-GHz CPU with 2 GB RAM. The modeling domain was divided by a rectangular grid with a cell size equal to $50 \times 50 \times 50$ m. Note that for INTEM3D code, we have to discretize a relatively large domain containing both bodies, A and B. The number of cells in this domain is 1536. Of course, one can use several integration domains in the framework of the conventional IE method [for example, SYSEM code can handle several integration domains (Xiong, 1992; Xiong and Kirsch, 1992)]. However, in the multidomain case, it is not possible to use an efficient fast Fourier transform (FFT) technique for fast matrix-vector multiplication. This is an important problem because without using the FFT, the computer memory requirements and the computational time increases dramatically. For example, SYSEM code would require many hours of computation for a model with just a few thousands cells, whereas INTEM3D code can handle up to 100,000 cells, typically within an hour, because INTEM3D code uses FFT, which requires just one integration domain. In the case of the inhomogeneous background method (IBCEM3D), we discretize separately the inhomogeneous part of the background (body B) and the anomalous domain (body A) and still use the FFT for each of these domains separately. For example, for Model 1, IBCEM3D uses 1024 cells because each body, A and B, contains 512 cells.

INTEM3D requires 862 s to compute the EM response for the model shown in Figure 2, whereas the IBC algorithm, IBCEM3D, does the same job in 1547 s. It takes more time to complete modeling with the new code because it involves two solutions of the linear system of IE: for body A and for body B. However, if we consider a homogeneous half-space and body B as inhomogeneous background and precompute and store the values of the variable background effect within body A, we can save significant computational time required for another modeling with the modified anomalous conductivity in body A. Furthermore, we could save computing time by using the stored fields when only the conductivity distribution within the anomalous domain is changed (body A) without a change of the domain geometry. For example, the computing time of the IBCEM3D algorithm becomes equal to 468 s at the second run of the code for the modified anomalous conductivity. Moreover, in real complex structures, the discretization grid covering the background inhomogeneities will be of an order larger than the grid covering the anomalous domain only. In this case, the conventional IE method will have to solve the system of linear equations on a large grid, whereas the new code, after precomputing the IBC field, will work only with the system of equation on a small grid. As a result, the computational time will reduce dramatically. An example of this time reduction for a typical geoelectrical model will be shown in the next section.

Model 2: Application to modeling the EM response of a sea-bottom petroleum reservoir in the presence of a salt dome structure

There is growing interest in the application of marine EM surveys for petroleum exploration. Zhdanov et al. (2004) investigated a typical model of an offshore sea-bottom petroleum reservoir in the presence of a salt dome structure. The IE modeling algorithm with IBC can be very useful in this modeling, especially when we have known information about the existence of a specific geologic structure, such as a salt dome. The model of a petroleum reservoir in the presence of a salt dome is one of the typical models in which the IBC modeling algorithm can be applied successfully. Figure 9 shows a sketch of this model (Model 2), which is similar to the one of Zhdanov et al., 2004.

The depth of the sea bottom is 500 m from the surface, and the seawater resistivity is equal to 0.3 ohm-m. The sea-bottom reservoir is approximated by a resistive rectangular body located 500 m below the sea bottom with a thickness of 100 m. The resistivity of the reservoir is 100 ohm-m, and the size of the reservoir is $5000 \times 5000 \times 100$ m^3. There is also a rectangular salt dome structure located close to the reservoir at a depth of 200 m below the sea bottom measuring $3000 \times 3000 \times 5000$ m^3. The resistivity of the salt dome is

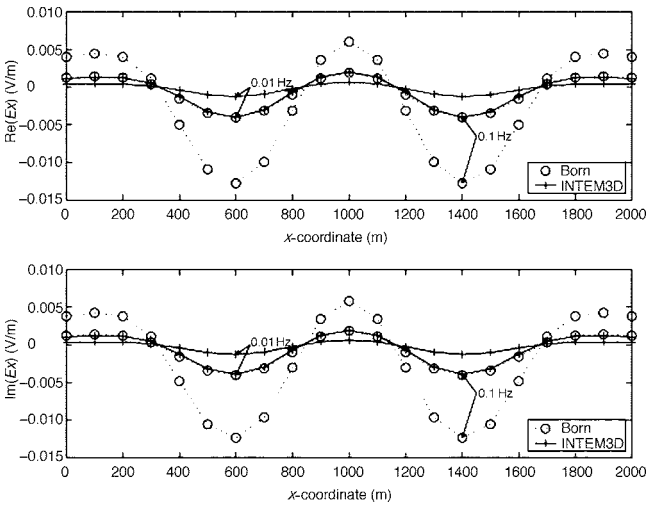

Figure 7. Plots of the real and imaginary parts of the sum of electric fields $E_x^{\Delta\sigma_b}$ and $E_x^{\Delta\sigma_a}$ along the x-directed profile at $y = 0$. The solid lines represent the results obtained by the conventional IE method (INTEM3D); the circles show the data computed using Born approximation.

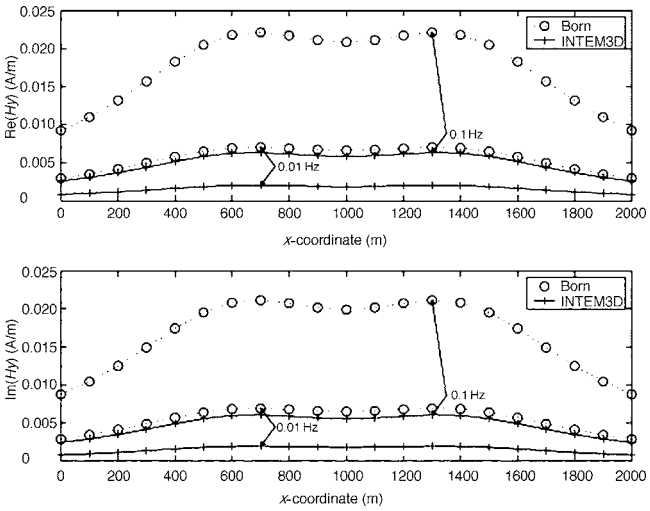

Figure 8. Plots of the real and imaginary parts of the sum of magnetic fields $H_y^{\Delta\sigma_b}$ and $H_y^{\Delta\sigma_a}$ along the x-directed profile at $y = 0$ calculated for Model 1. The solid lines represent the results obtained by INTEM3D; the circles show the data computed by Born approximation.

Downloaded 12/18/15 to 132.239.1.230. Redistribution subject to SEG license or copyright; see Terms of Use at http://library.seg.org/

30 ohm-m. The model is excited by a vertically propagated plane EM wave with eight frequencies: 0.0003, 0.001, 0.003, 0.01, 0.03, 0.1, 0.3, and 1 Hz.

We have applied both algorithms, the conventional IE method and the new code, to generate an EM field for this model in 572 receivers located every 500 m on a 26×22 grid at the sea bottom. The anomalous body is divided into rectangular cells with a square horizontal section, 500×500 m^2, and with the vertical size increasing with the depth as follows: 100, 100, 100, 100, 100, 100, 100, 300, 1000, and 3000 m. The total number of cells is 1980 in the conventional INTEM3D code, which requires the discretization of the entire domain containing both the reservoir and the salt dome. The IBCEM3D requires the discretization of the salt dome domain and of the reservoir domain only. We use 360 cells to represent a salt dome and 100 cells for a reservoir.

Using the IBCEM3D code, however, we combine the 1D model of the sea layer and the sea-bottom sediments and a salt dome structure in one inhomogeneous background. In this case, we only need 360 cells for a salt dome and 100 cells for a reservoir, 460 cells total.

Figures 10 and 11 compare the E_x- and H_y-components computed using two different codes for the x-directed profile at $y = -1250$ m. The solid lines represent the results obtained by the conventional IE method (INTEM3D); the circles represent those computed using a new inhomogeneous background algorithm (IBCEM3D). One can see that the two results almost match each other.

Table 2 presents the results of the accuracy analysis of the IBC method for this model based on formulas 16 and 17. Note that we evaluate the accuracy of the IBC IE method in comparison with the conventional IE method.

The relative errors ε_1^b and ε_1^a do not exceed 0.3% for H-polarization and 0.1% for E-polarization, respectively.The errors are slightly larger for H-polarization than for E-polarization. The errors of the IBC method decrease with the frequency because galvanic coupling between a salt dome and a reservoir, which is the strongest source of the IBC errors in this case, decreases with the frequency.

Computing time for this modeling was evaluated in a Matlab 7.0 environment on the same PC equipped with Intel Pentium 4 3.6-GHz CPU and 2-GB RAM as for Model 1. The conventional IE modeling method (INTEM3D code) required 828 s for this model. The inhomogeneous background modeling algorithm (IBCEM3D), however, required 523 s. Assuming that the boundaries of the anomalous domain containing the reservoir are fixed but only the conductivity distribution varies, we can perform another modeling within 7 s

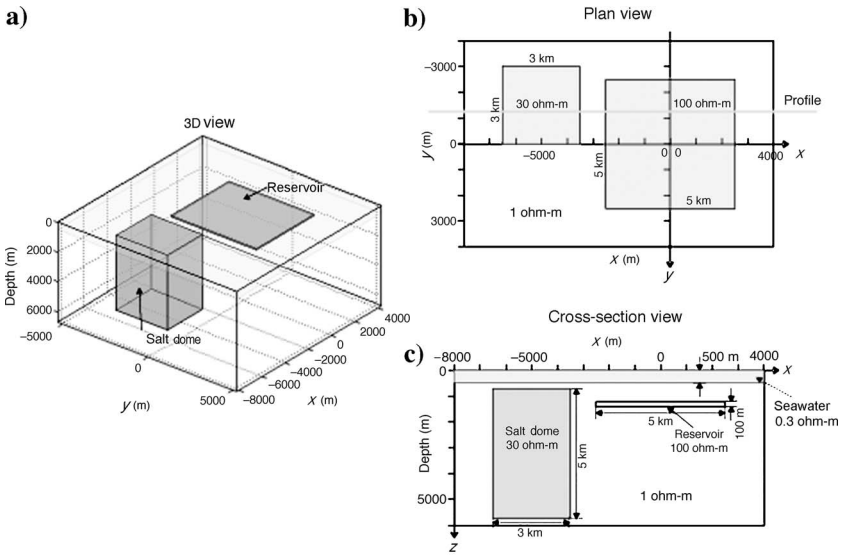

Figure 9. A sketch of Model 2 of an offshore sea-bottom petroleum reservoir in the presence of a salt dome structure. (a) 3D view, (b) a plan view, and (c) vertical cross section of Model 2.

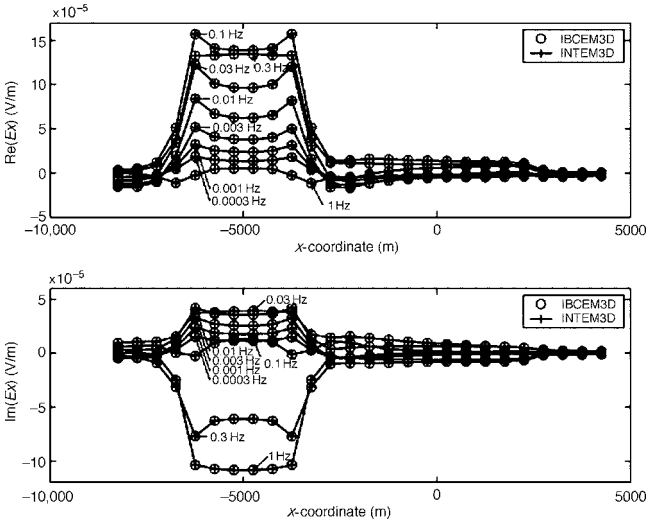

Figure 10. Model 2. Plots of the real and imaginary parts of the sum of electric fields $E_x^{\Delta\sigma_b}$ and $E_x^{\Delta\sigma_a}$ along the x-directed profile at $y = 1250$ m. The solid lines represent the results obtained by INTEM3D; the circles show the data computed by IBCEM3D.

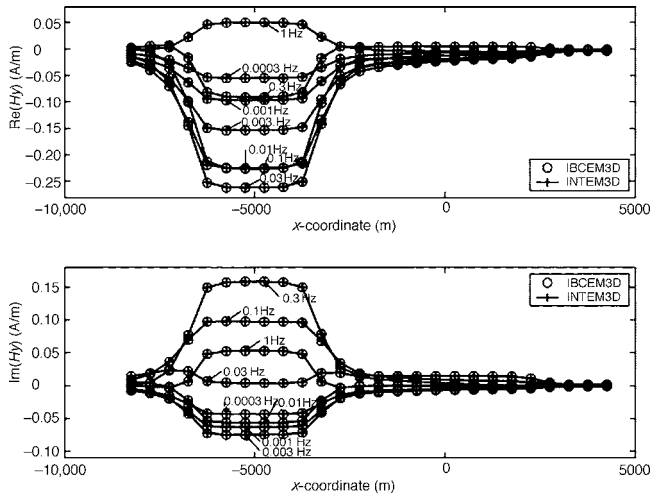

Figure 11. Model 2. Plots of the real and imaginary parts of the sum of magnetic fields $H_x^{\Delta\sigma_b}$ and $H_x^{\Delta\sigma_b}$ along the x-directed profile at $y = -1250$ m. The solid lines represent the results obtained by INTEM3D; the circles shows the data computed by IBCEM3D.

Downloaded 12/18/15 to 132.239.1.230. Redistribution subject to SEG license or copyright; see Terms of Use at http://library.seg.org/

Table 2. Accuracy of IBC IE method for Model 2.

Frequency Hz	ε_1^b H-pol.	ε_1^b E-pol.	ε_1^a H-pol.	ε_1^a E-pol.
0.001	0.0021	0.0010	0.0034	0.0005
0.01	0.0018	0.0013	0.0030	0.0005
0.1	0.0011	0.0012	0.0016	0.0002
1	0.0004	0.0004	0.00001	0.00002

in this example. This is a very effective and powerful result, which may be especially useful in inversion analysis, which requires numerous forward modelings.

Model 3: A sea-bottom petroleum reservoir attached to a salt dome structure

To investigate more carefully the practical limitations of the IBC IE method, we consider Model 3, which is similar to Model 2 (Figure 9), but the petroleum reservoir is now attached to the salt dome as shown in Figure 12. We should note, however, that the simulated attachment may not represent real (physical) attachment, just because discretization tends to disconnect the bodies even if they are meant to be connected. However, this is a typical limitation for any numerical modeling.

The model is excited by a vertically propagated plane EM wave with eight frequencies: 0.0003, 0.001, 0.003, 0.01, 0.03, 0.1, 0.3, and 1 Hz. We have used the same discretization for Model 3 as for Model 2 and applied both algorithms, the conventional IE method and the new IBC IE method, to generate an EM field for this model.

Figures 13 and 14 show the comparisons of the E_x- and H_y components, computed using two different codes for the x-directed profile at $y = -1250$ m. The solid lines represent the results obtained by the INTEM3D code; the circles represent those computed using the new inhomogeneous background IBCEM3D algorithm. Once again, we can see that the two results are very close to each other. However, the results of the accuracy analysis, presented in Table 3, show that the relative errors increase for Model 3 in comparison with Model 2 (Table 2). As we can see from Table 3, the relative errors of the IBC IE solution for H-polarization do not exceed 10% within a salt dome domain (ε_1^b), and 14% within a

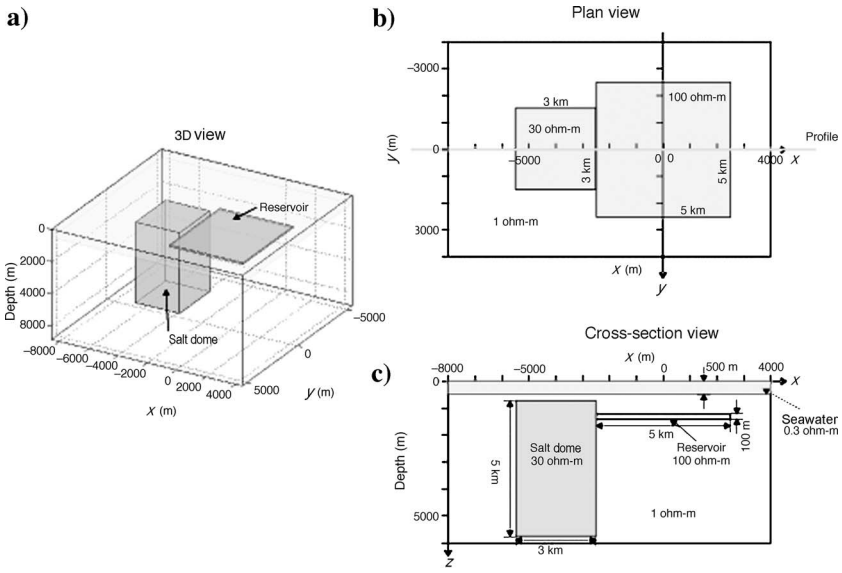

Figure 12. A sketch of Model 3 of an offshore sea-bottom petroleum reservoir attached to a salt dome structure. (a) 3D view, (b) plan view, and (c) vertical cross section of Model 3.

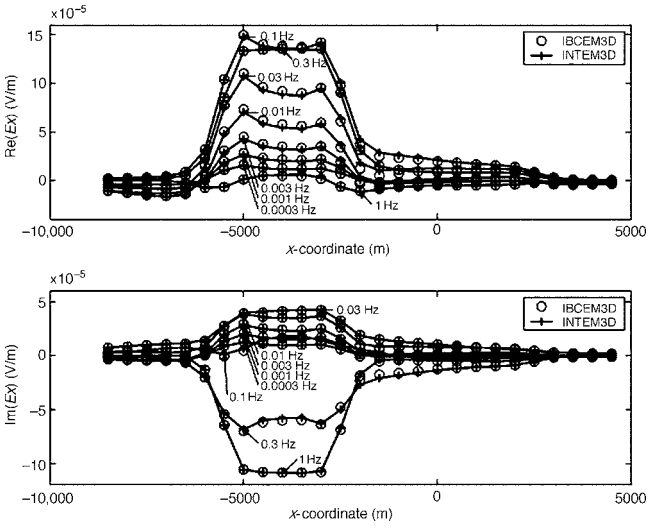

Figure 13. Model 3. Plots of the real and imaginary parts of the sum of electric fields $E_x^{\Delta\sigma_b}$ and $E_x^{\Delta\sigma_a}$ along the x-directed profile at $y = 1250$ m. The solid lines represent the results obtained by INTEM3D; the circles show the data computed by IBCEM3D.

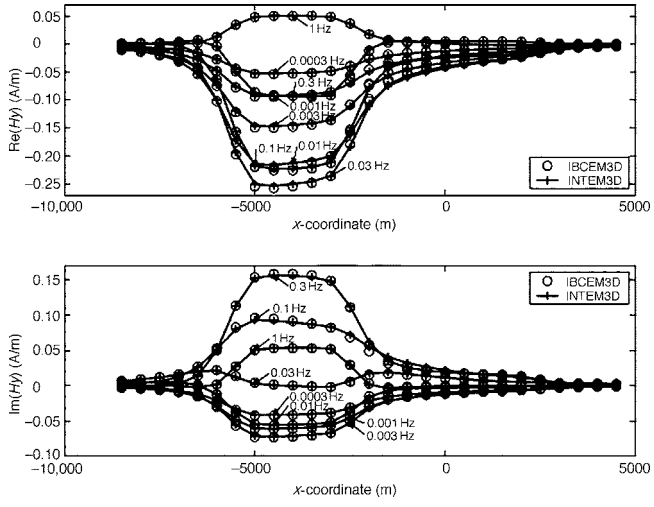

Figure 14. Model 3. Plots of the real and imaginary parts of the sum of magnetic fields $H_x^{\Delta\sigma_b}$ and $H_x^{\Delta\sigma_b}$ along the x-directed profile at $y = -1250$ m. The solid lines represent the results obtained by INTEM3D; the circles shows the data computed by IBCEM3D.

Downloaded 12/18/15 to 132.239.1.230. Redistribution subject to SEG license or copyright; see Terms of Use at http://library.seg.org/

Table 3. Accuracy of IBC IE method for Model 3.

Frequency Hz	ε_1^b H-pol.	ε_1^b E-pol.	ε_1^a H-pol.	ε_1^a E-pol.
0.001	0.107	0.010	0.142	0.020
0.01	0.095	0.009	0.141	0.016
0.1	0.068	0.006	0.147	0.011
1	0.040	0.006	0.152	0.009

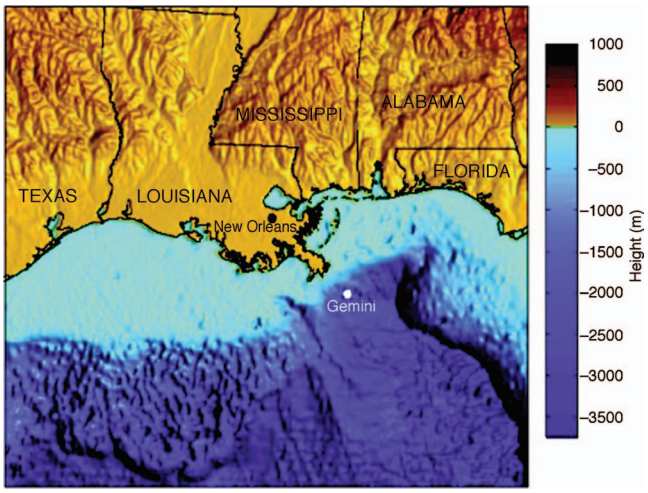

Figure 15. Location of Gemini Prospect, Gulf of Mexico. Topography and bathymetry from Smith and Sandwell, 1997.

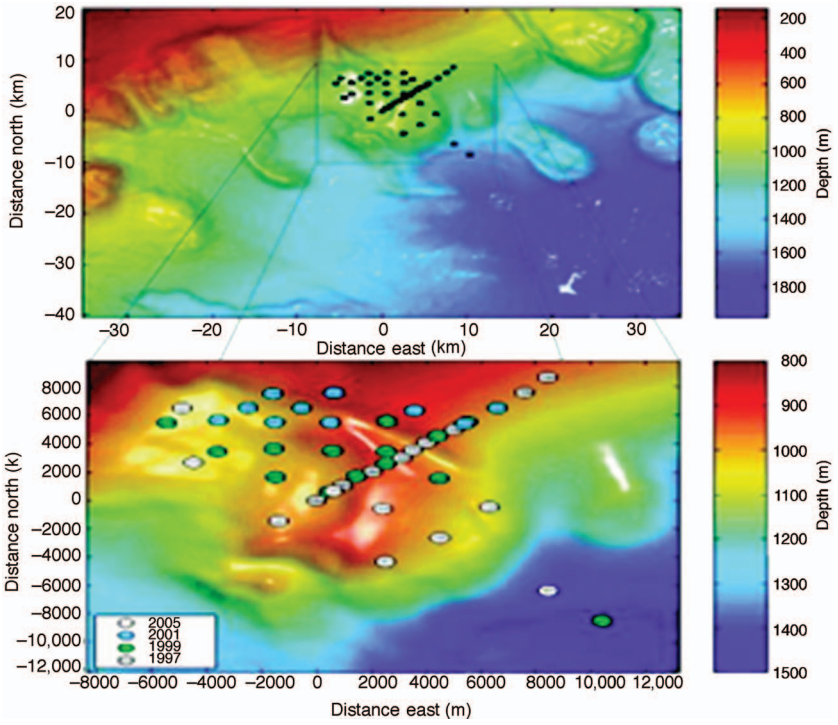

Figure 16. Bathymetry and the MT site locations at Genimi Prospect (after Key, 2003).

reservoir domain (ε_1^a), respectively. The corresponding relative errors of the IBC IE solution for E-polarization are smaller. They do not exceed 1% within a salt dome domain, and 2% within a reservoir domain, respectively. The errors are significantly larger for H-polarization than for E-polarization because the galvanic interaction between the salt dome and an attached reservoir are stronger for H-polarization than for E-polarization. Note again that the accuracy of the IBC IE method is evaluated in comparison with the conventional IE method.

Computing time for this modeling was evaluated on the same PC, as that for Model 2. The INTEM3D code required 653 s for this model. The IBCEM3D code, however, required 523 s. However, additional modeling for updated anomalous conductivity distribution within the reservoir domain only requires just an extra 7 s per model.

APPLICATION OF THE IBC IE METHOD TO STUDY THE BATHYMETRY EFFECTS IN MCSEM DATA: GEMINI PROSPECT MODEL

In this section, we present an application of the IBC IE method for modeling the bathymetry effects in the MCSEM data. We consider a practical case of modeling the MCSEM data in the Gemini Prospect area, located about 200 km southeast of New Orleans in the deep water northern Gulf of Mexico (Figure 15). The Gemini salt body lies 1.5 km beneath the sea floor in 1 km water depth and has a high electrical resistivity compared with the surrounding sediments, making it a suitable target for electrical methods. The subsalt gas deposit at Gemini is located at a depth of about 4 km on the southeastern edge of the Gemini structure (Ogilive and Purnell, 1996). The Scripps Institution of Oceanography conducted several sea-bottom MT surveys in Gemini Prospect in 1997, 1998, 2001, and 2003 at 42 MT sites (Figure 16). A detailed analysis of the Gemini MT data, using 2D Occam's inversion, was presented by Key (2003) and Key et al. (2006).

Zhdanov et al. (2004) and Wan et al. (2006) conducted a 3D inversion of the MT data collected at Gemini Prospect and produced a 3D geoelectrical model of a salt dome structure in this area. Figure 17 shows a typical vertical section of the geoelectrical model obtained by 3D inversion. The depth of the sea bottom is about 1 km from the surface, and the seawater resistivity is 0.3 ohm-m. We have included in this geoelectrical model the detailed bathymetry data provided by the Scripps Institution of Oceanography (Figure 16).

The EM field in this model is generated by a horizontal electric dipole (HED) transmitter with a length of 100 m and located at $(x, y) = (0, 0)$ km at a depth of 50 m above the sea bottom. The transmitter generates the EM field with a transmitting current of 1 A at 0.25 Hz. Note that, in practice, the transmitting current may be equal to 100 A or even to 1 KA. However, the observed data are usually normalized by the current in the transmitter. An array of seafloor electric receivers is located 5 m above the sea bottom along a line

Downloaded 12/18/15 to 132.239.1.230. Redistribution subject to SEG license or copyright; see Terms of Use at http://library.seg.org/

with the coordinates ($x = \{-2, 10\}$ km, $y = 0$) with a spacing of 0.5 km (Figure 18).

We have computed the electric field in this model using three different techniques: the IBC IE method, the iterative IBC method, and the conventional IE method. Note that in the previous section, we examined the IBC IE method using the IBCEM3D modeling code (Zhdanov and Lee, 2005), which was an extension of the original INTEM3D code (Hursán and Zhdanov, 2002). In the current section, we use another software developed using the IBC IE method, which is based on an extension of the parallel integral equation PIE3D software of Yoshioka and Zhdanov (2005). Modeling the bathymetry effects requires using large discretization grids, and PIE3D software is more suitable for solving large numerical problems than is the original INTEM3D code. The computations were conducted in 64-bit Linux environment with two AMD Opteron 246 (2.0-GHz) CPUs with 4 GB RAM.

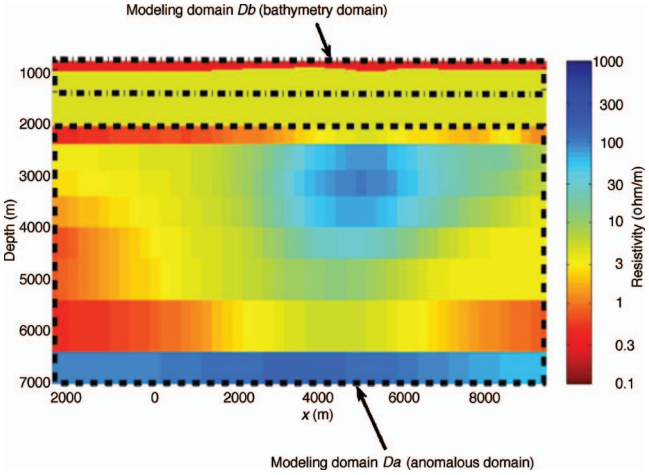

Figure 17. A typical vertical section of the geoelectrical model obtained by 3D inversion of marine MT data in the Gemini Prospect area (after Wan et al., 2006).

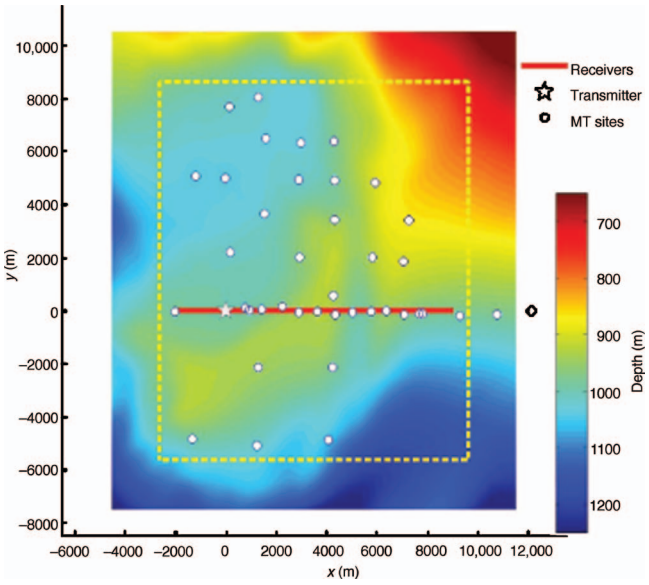

Figure 18. A bathymetry map for the Gemini Prospect area. A dashed yellow rectangular line outlines the modeling domain of the salt dome geoelectrical structure. A bold red horizontal line shows the position of the MCSEM profile. A horizontal electric bipole oriented in the x-direction is located at a point with horizontal coordinates $x = 0$ m, and $y = 0$ m at a depth 50 m above the sea bottom.

First of all, we applied the IBC method. Following the main principales of the IBC IE method, the modeling area was represented by two modeling domains, D_a and D_b, outlined by the black dashed lines in Figure 17. Modeling domain D_b covers the area with conductivity variations associated with the bathymetry of the sea bottom, whereas modeling domain D_a corresponds to the location of the salt dome structure obtained by 3D inversion of the MT data. We used 99,645 ($65 \times 73 \times 21$) cells with each cell size $250 \times 250 \times 25$ m^3 for a discretization of the bathymetry structure. The domain D_a of the salt dome area was discretized in 22,344 ($49 \times 57 \times 8$) cells with the same horizontal size, 250 m $\times$ 250 m, and with a variable vertical size, starting with 350 m and progressively increasing with depth up to 1000 m.

The second round of computations was fulfilled using the iterative IBC. Figure 19 presents the convergence plot for iterative IBC modeling. One can see that it takes just three iterations to reach a relative error below excess 1×10^{-8} in the salt dome domain and in the bathymetry domain. We can see from the same plots that the relative errors of the original IBC solution (the first iteration of the iterative method) are about 0.01%. Naturally, these small errors within the modeling domain transform into even smaller errors in the computed data in the receivers. Indeed, one cannot notice any difference between the two modeling results in the amplitude-versus-offset (AVO) plot of the observed inline electric field data shown in Figure 20. For comparison, we present in the same figure the results of the numerical modeling produced by a standard IE forward modeling software, PIE3D.

Figure 21a shows the AVO plots of the total inline electric field, normalized by the amplitude of the background field (which includes a bathymetry effect in this case), computed using all three different numerical techniques. The normalized differences between the IBC and iterative IBC results and a conventional IE solution are shown in Figure 21b. One can see that the errors of the IBC solution

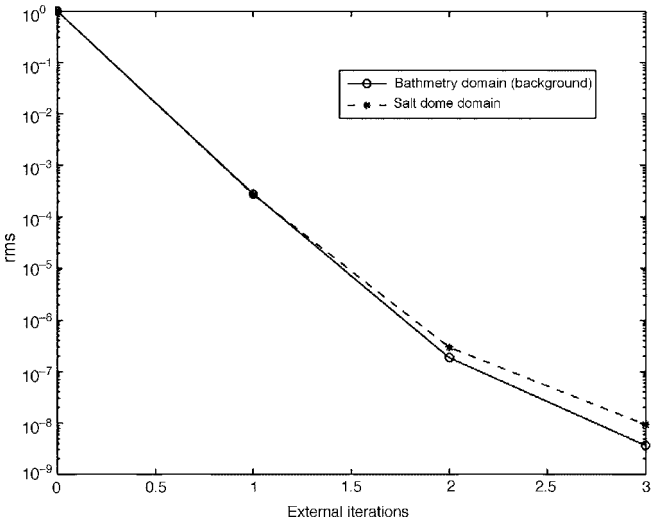

Figure 19. Gemini Prospect model. The convergence plot for iterative IBC modeling. The solid line with circles shows the relative errors versus iteration number for the inhomogeneous background (bathymetry) domain; the dashed line with asterisks presents the same curve for the anomalous (salt dome) modeling domain.

Downloaded 12/18/15 to 132.239.1.230. Redistribution subject to SEG license or copyright; see Terms of Use at http://library.seg.org/

do not exceed 3%, whereas the errors of the iterative method are practically the same as the accuracy of the conventional IE solution (0.002%). This result demonstrates that the developed technique produces an extremely accurate result even in the complex case of the inhomogeneous background formed by the bathymetric effects associated with the conductivity contrast between the saltwater and the sea-bottom sediments.

Computing time for this modeling was evaluated in 64-bit Linux environment with two AMD Opteron 246 (2.0-GHz) CPUs with 4 GB RAM. The conventional IE modeling by PIE3D code required 462 s for this model. The IBC algorithm required 337 s. Additional modeling for updated anomalous conductivity distribution within the salt dome domain only requires just an extra 92 s per model. The iterative IBC algorithm is not optimized yet. It took 836 s for this model, which is still very fast.

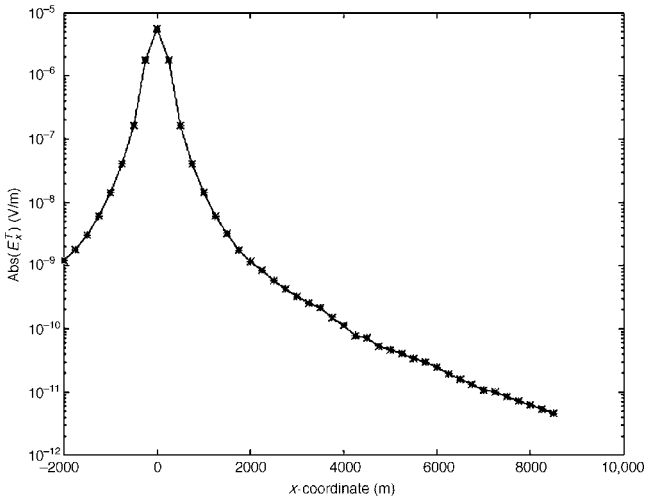

Figure 20. AVO plots of the observed inline electric field data for the Gemini Prospect model obtained using the IBC IE method, the iterative IBC method (crosses), and the conventional IE method (solid line).

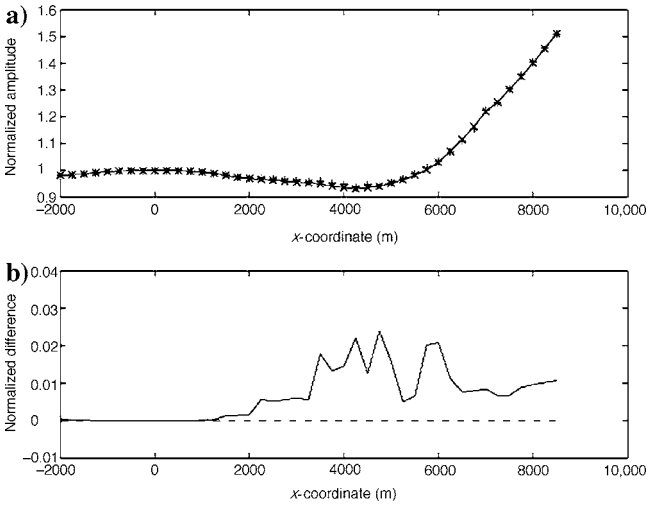

Figure 21. Synthetic MCSEM data computed for the Gemini Prospect geoelectrical model. (a) The AVO plots of the total inline electric field normalized by the amplitude of the background field along an MCSEM profile. The pluses show the results obtained by the IBC method, the crosses present the same data computed by the iterative IBC approach, and the solid line presents the result obtained by a conventional IE method. (b) Normalized differences between the IBC and a conventional IE solution (solid line) and between the iterative IBC and a conventional IE solution results (dashed line).

CONCLUSIONS

The results of this paper clearly demonstrate that the IE method can be formulated not only for models with a horizontally layered background but also for those with a variable background conductivity. However, this new formulation can still use the same layered-earth Green's function as the conventional IE method. This fact opens the possibility of incorporating an inhomogeneous background, such as a known geologic structure or the terrain and bathymetry effects, in IE-based forward modeling.

The accuracy of the IBC IE method depends on the electrical distance between a domain with the IBC and an anomalous domain. The larger this distance, the smaller the return effect of the currents induced in the anomalous domain on the IBC domain and vice versa. However, our modeling study shows that even in the case of the anomalous domain (e.g., petroleum reservoir) attached to the IBC domain (e.g., a salt dome structure), we still have good accuracy with the IBC IE method.

To provide a quantitative evaluation of the accuracy of the IBC IE technique, we have developed a method of accuracy control based on evaluation of errors related to ignoring the return response of the currents induced in the inhomogeneous background on the field in the anomalous domain. In addition, we have presented an iterative version of the IBC IE technique that actually provides a rigorous solution of the forward modeling problem.

We have applied a new IBC IE method for modeling the MCSEM data in the areas with significant bathymetric inhomogeneities. The main difficulties of modeling EM fields for complex sea-bottom structures in the presence of rough bathymetry are because we need to use a large number of discretization cells to adequately present the complex relief of the seafloor structure. Application of the IBC EM method allows us to separate this computational problem into at least two problems with relatively smaller sizes.

Another advantage of the IBC IE method that is even more important in practical applications is related to the fact that interpretation of the field data usually requires multiple solutions of the forward problem with different parameters of the target (in our examples, a salt dome structure or a sea-bottom hydrocarbon reservoir). The traditional IE method would require repeating these massive computations, including hundreds of thousands of cells covering the bathymetry, every time we change the model of the target, which is extremely expensive. At the same time, using the IBC approach, we can precompute the bathymetry effect only once and then repeat the computations on a smaller grid covering the anomalous domain only. The last factors may prove to be critical in the effective use of the IE method in fast EM inversion over complex geoelectrical structures.

ACKNOWLEDGMENTS

The authors acknowledge the support of the University of Utah Consortium for Electromagnetic Modeling and Inversion (CEMI), which includes BAE Systems, Baker Atlas Logging Services, BGP China National Petroleum Corporation, BHP Billiton World Exploration Inc., Centre for Integrated Petroleum Research, EMGS, ENI S.p.A., ExxonMobil Upstream Research Company, INCO Explora-

tion, Information Systems Laboratories, MTEM, Newmont Mining Co., Norsk Hydro, OHM, Petrobras, Rio Tinto-Kennecott, Rocksource, Schlumberger, Shell International Exploration and Production Inc., Statoil, Sumitomo Metal Mining Co., and Zonge Engineering and Research Organization.

We are thankful to Steve Constable and Kerry Key of the Scripps Institution of Oceanography for providing the real bathymetry and MT data for Gemini prospect area.

Seong Kon Lee was supported by the Development of Deep, Low-enthalpy Geothermal Energy project, funded by KIGAM and the post-doctoral fellowship program funded by Korea Science and Engineering Foundation KOSEF.

REFERENCES

Abubakar, A., and P. M. van der Berg, 2004, Iterative forward and inverse algorithms based on domain integral equations for three-dimensional electric and magnetic objects: Journal of Computational Physics, **195**, 236–262.

Avdeev, D. B., 2005, Three-dimensional electromagnetic modelling and inversion from theory to application: Surveys in Geophysics, **26**, 767–799.

Avdeev, D. B., A. V. Kuvshinov, O. V. Pankratov, and G. A. Newman, 2002, Three-dimensional induction logging problems, Part I: An integral equation solution and model comparisons: Geophysics, **67**, 413–426.

Dmitriev, V. I., 1969, Electromagnetic fields in inhomogeneous media: Proceedings of the Computational Center, Moscow State University (in Russian).

Dmitriev, V. I., and N. I. Nesmeyanova, 1992, Integral equation method in three-dimensional problems of low-frequency electrodynamics: Computational Mathematics and Modeling, **3**, 313–317.

Hohmann, G. W., 1975, Three-dimensional induced polarization and electromagnetic modeling: Geophysics, **40**, 309–324.

Hursán, G., and M. S. Zhdanov, 2002, Contraction integral equation method in three-dimensional electromagnetic modeling: Radio Science, **37**, 61089, doi 10.1029/2001RS002513.

Key, K. W., 2003, Application of broadband marine magnetotelluric exploration to a 3D salt structure and a fast spreading ridge: Ph.D. thesis, University of California, San Diego.

Key, K. W., S. C. Constable, and C. J. Weiss, 2006, Mapping 3D salt using the 2D marine magnetotelluric method: Case study from Gemini Prospect, Gulf of Mexico: Geophysics, **71**, B17–B27.

Ogilive, J. S., and G. W. Purnell, 1996, Effects of salt related mode conversions on subsalt prospecting: Geophysics, **61**, 331–348.

Raiche, A. P., 1974, An integral equation approach to three-dimensional modelling: Geophysical Journal of the Royal Astronomical Society, **36**, 363–376.

Singer, B. S., and E. B. Fainberg, 1997, Fast and stable method for 3D modeling of electromagnetic field: Exploration Geophysics, **28**, 130–135.

Singer, B. S., A. Mezzatesta, and T. Wang, 2003, Integral equation approach based on contraction operators and Krylov subspace optimisation, *in* J. Macnae and G. Liu, eds, Three-dimensional electromagnetics III: Australian Society of Exploration Geophysicists.

Smith, W. H. F., and D. T. Sandwell, 1997, Global seafloor topography from satellite altimetry and ship depth soundings: Science, **277**, 1956–1962.

Tabarovsky, L. A., 1975, Application of integral equation method to geoelectrical problems: Nauka (in Russian).

Wan, L., M. S. Zhdanov, K. Key, and S. Constable, 2006, Rigorous 3D inversion of marine MT data: Proceedings of Annual Meeting, Consortium for Electromagnetic Modeling and Inversion, 229–254.

Wannamaker, P. E., 1991, Advances in three-dimensional magnetotelluric modeling using integral equations: Geophysics, **56**, 1716–1728.

Weidelt, P., 1975, Electromagnetic induction in three-dimensional structures: Journal of Geophysics, **41**, 85–109.

Xiong, Z., 1992, Electromagnetic modeling of 3D structures by the method of system iteration using integral equations: Geophysics, **57**, 1556–1561.

Xiong, Z., and A. Kirsch, 1992, Three-dimensional earth conductivity inversion: Journal of Computational and Applied Mathematics, **42**, 109–121.

Yoshioka, K., and M. S. Zhdanov, 2005, Electromagnetic forward modeling based on the integral equation method using parallel computers: 75th Annual International Meeting, SEG, Expanded Abstracts, 550–553.

Zhdanov, M. S., 2002, Geophysical inverse theory and regularization problems: Elsevier Scientific Publ., Inc.

Zhdanov, M. S., and S. K. Lee, 2005, Integral equation method for 3D modeling of electromagnetic fields in complex structures with inhomogeneous background conductivity in marine CSEM applications: 75th Annual International Meeting, SEG, Expanded Abstracts, 510–513.

Zhdanov, M. S., L. Wan, S. Constable, and K. Key, 2004, New development in 3D marine MT modeling and inversion for off-shore petroleum exploration: 74th Annual International Meeting, SEG, Expanded Abstracts, 588–591.

Zhdanov, M. S., and G. A. Wilson, 2004, 3D inversion of electromagnetic data based on the quasi-analytical approximation for inhomogeneous background conductivity: 74th Annual International Meeting, SEG, Expanded Abstracts, 692–695.

Downloaded 12/18/15 to 132.239.1.230. Redistribution subject to SEG license or copyright; see Terms of Use at http://library.seg.org/